PCCP

Accepted Manuscript

ROYAL SOCIETY OF CHEMISTRY

www.rsc.org/pccp

Electrochemistry of orthosilicate-based lithium battery cathodes: a perspective

Stefania Ferrari[a*], Doretta Capsoni[a], Simone Casino[b], Matteo Destro[b], Claudio Gerbaldi[b], Marcella Bini[a]

[a] Department of Chemistry, University of Pavia, viale Taramelli 16, 27100 Pavia (Italy)

[b] GAME Lab, Department of Applied Science and Technology - DISAT, Institute of Chemistry, Politecnico di Torino, Corso Duca degli Abruzzi 24, 10129 Torino (Italy)

Corresponding Author
* stefania.ferrari@unipv.it
S.Ferrari@warwick.ac.uk
Department of Chemistry, University of Pavia
viale Taramelli 16,
27100 Pavia, Italy
Phone: 39-382-987213; FAX: 39-382-987575

TOC

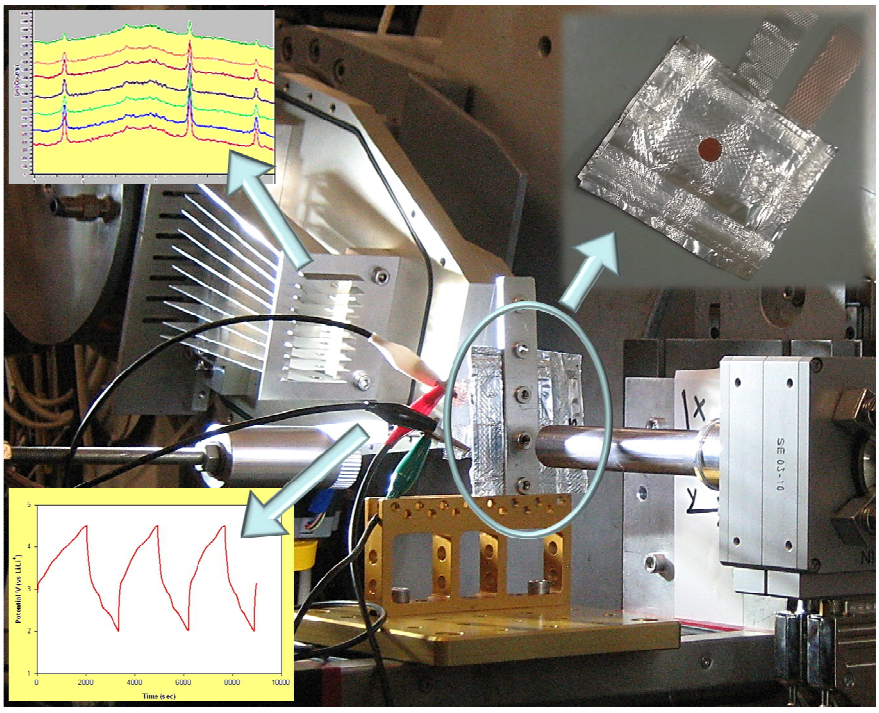

In this perspective we highlight the electrochemical features of lithium metal orthosilicates, investigated by combined *in* or *ex situ* XRD and electrochemical measurements.

Abstract

Lithium metal orthosilicates are attracting a lot of attention owing to their promising prospects as potential high capacity cathode materials for Li-ion batteries. Currently, great efforts are being made in order to reach the full theoretical specific capacity of 330 mAh g^{-1}, but many issues remain unsolved (e.g., poor structural and cycling stability) which limit the practical application. The present perspective highlights the importance of assessing the electrochemical behaviour of $Li_2(Fe,Mn)SiO_4$ by combining an arsenal of characterization technique both spectroscopic and structural, *in* and *ex* situ. We are here reviewing the most recent achievements in the investigation of the electrochemical performance of lithium metal orthosilicate cathodes and, through some of our recent results, attempting to clarify the relationship between structure and electrochemistry of these compounds.

Keywords

Li_2FeSiO_4, *in situ* X-ray diffraction, synchrotron radiation, cathode, lithium battery

1- **Introduction**

In the on-going search for novel, high performing, green and safe positive electrode materials for the next-generation of Li-ion secondary batteries, lithium transition metal orthosilicates have attracted newfound attention [1,2]. Their formula is Li_2MSiO_4 (where M = Mn, Fe or a mixture thereof) for which, in principle, the extraction of 2 Li^+ ions per formula unit is possible thus resulting in a 2-electron process and, correspondingly, an enhanced energy density. The properties of these materials have been extensively studied and, in particular, their structural features are now well known [3,4]: they show a rich polymorphism, including monoclinic and orthorhombic structures stable in different temperature intervals. The study of the polymorphs was often performed by combining diffraction, microscopic and spectroscopic techniques, to obtain information on both long and short range ordering of the polyoxyanion framework. Among the diffraction techniques, X-ray powder diffraction (XRD) has been extensively used, both in house or by using Synchrotron radiation, while ^{6,7}Li Magic Angle Spinning Nuclear Magnetic Resonance (MAS NMR) [5-7], ^{57}Fe Mössbauer [6, 8] and X-ray Absorption Spectroscopy/ X-ray Absorption Near Edge Spectroscopy (XAS/XANES) [9,10] revealed to be powerful spectroscopic tools to precisely ascertain the crystal structure and to investigate the oxidation state of Fe atoms. Transmission Electron Microscopy (TEM) in combination with electron diffraction was also used to describe the crystal chemistry of the orthosilicate family [11,12].

The well known structures for Li_2FeSiO_4 are: the *Pmn2*$_1$, the *P2*$_1$*/n* and the *Pmnb* (see Figure 1), stable at low, intermediate and high temperatures, respectively. The *Pmn2*$_1$ structure may be easily obtained by hydrothermal synthesis at about 200 °C, while the monoclinic or orthorhombic crystal systems can be stabilised depending on the annealing temperature, but also on the synthesis method and on the presence of polymeric surfactants used for carbon coating [10,13]. In some cases a mixture of polymorphs was observed, due to the similar formation energy of the different structures. In the case of mixed $Li_2Fe_{1-x}Mn_xSiO_4$ compounds, depending both on the composition and the synthesis temperature, the co-presence of different polymorphs was reported [4]. In particular, the *Pmn2*$_1$ and *P2*$_1$*/n* polymorphs were found to coexist at 700 °C for the $Li_2Fe_{0.5}Mn_{0.5}SiO_4$ composition [4]. Other works showed the formation of the single phase *Pmn2*$_1$ polymorph in the temperature range of 600-700 °C [14-16]. In a previous work [17], we showed a mixed $Li_2Fe_{0.5}Mn_{0.5}SiO_4$ having the *Pmnb* structure, which was prepared at 650 °C and demonstrated to be the stable phase up to 950 °C by means of *in situ* XRD analysis. The anti-site defect involving Li and Fe ions exchange was found to increase by increasing the temperature, reaching a high value at 950 °C [17]. The formation of disordered structures such as the *Pmn2*$_1$

having anti-site defect, namely inverse β_{II}, was observed in electrodes analyzed after cycling in lithium cell [18].

The magnetic properties of Li_2FeSiO_4 were reported and discussed in different studies [1,7,19,20]. An antiferromagnetic ordering with a Neel temperature (T_N) of 24 K [20] or 20 K [1, 7, 19] was detected, due to the different amount of Fe^{3+} atoms in the silicate structure. In fact, a second T_N of 28 K was observed for a partially delithiated sample [19], thus suggesting that the higher is the T_N value, the higher the Fe^{3+} content. Therefore, a T_N of 20 K indicates that Fe is mostly present in the (2+) oxidation state. Another important property of Li_2FeSiO_4 to be considered for its application as lithium battery cathode is the specific conductivity. It was found to be around 6×10^{-14} S cm^{-1} at ambient temperature, which accounts for the almost insulating properties of this electrode material [21]. In this respect, the preparation of nanoscale particles particularly in the form of composites with an electron-conducting phase revealed to be of paramount importance for its practical application.

The fundamental studies on the crystal structure and properties of the orthosilicate family reported above constitute the basic knowledge for a thorough comprehension of its electrochemical behavior upon cycling in lithium cell. In 2007, Dominko and co-workers discussed the electrochemical characteristics of Li_2FeSiO_4 and Li_2MnSiO_4, evidencing the dramatic decay in terms of specific capacity and efficiency during cycling. This was particularly evident for the Mn-based compound [22,23], due to its irreversible amorphization. As a consequence, the present worldwide research has been focused on the understanding of this behaviour. The theoretical capacity of about 330 mAh g^{-1} has not been reached so far, and several aspects deserve to be clarified, including the iron/manganese oxidation steps, the structure of the delithiated phases and the formation of defects during cycling. At present, Li_2FeSiO_4 and Li_2MnSiO_4 are mostly investigated to unravel their electrochemical features, but the mixed iron/manganese silicates were suggested as a possible solution for reducing the irreversible amorphization of the pristine Li_2MnSiO_4 structure upon cycling [23].

In the present perspective, the attention is polarized on the investigation of the electrochemical cycling behaviour in lithium cell of both Li_2FeSiO_4 and $Li_2Fe_{0.5}Mn_{0.5}SiO_4$ compounds. Theoretical works are discussed as well as experimental studies based on conventional characterization techniques such as cyclic voltammetry, galvanostatic charge/discharge measurements and Galvanostatic and Potentiostatic Intermittent Titration Techniques (GITT and PITT). The most recent results both from *ex* and *in situ* structural/spectroscopic studies directed to a deeper understanding of the electrochemical features of these compounds are reviewed. In addition, we discuss our experimental results recently obtained by Synchrotron XRD analysis of both monoclinic

Li_2FeSiO_4 and orthorhombic $Li_2Fe_{0.5}Mn_{0.5}SiO_4$, carried out *in situ* during cycling in lithium cell to highlight any difference in the behaviour of the two different polymorphs. A Li_2FeSiO_4 sample having a disordered structure was also prepared for the first time, and the results of the *in situ* XRD analysis during cycling are hereby compared with those of the ordered one, also based on the recent literature reports.

2- Electrochemistry of Li_2FeSiO_4 and $Li_2Fe_{0.5}Mn_{0.5}SiO_4$

2.1 - Theoretical calculations

This paragraph is not intended to be a comprehensive review of the theoretical works present in the literature. In fact, only the most recent findings are discussed, as the present perspective article is mainly focused on the thorough discussion of experimental data. Many theoretical studies were reported based on both Density Functional Theory (DFT) and first principle calculations. They show the behaviour of Li_2FeSiO_4 and $LiFeSiO_4$ upon lithium extraction, trying to define the Fe oxidation potential, the energy of the crystal structures obtained upon delithiation and the migration pathways of the Li^+ ions. These investigations often compare the different polymorphs by calculating their total energy, with the aim of determining the most stable structure for both the partially $LiFeSiO_4$ and the fully delithiated $FeSiO_4$ compounds. Independently of the initial structure ($P2_1/n$, $Pmn2_1$ or Pmnb), the energy differences among the resulting $LiFeSiO_4$ polymorphs were found to be relatively large upon extraction of one Li^+ ion and the phase transformation towards the inverse β_{II} phase seemed to be preferred (see Figure 2) [24]. In fact, this study pointed out that structures of polymorphs having a 3D framework, such as the inverse $Pmn2_1$, are more stable compared with two dimensional ones. Many studies evidenced the low energy variation upon delithiation of the inverse β_{II} phase as well as the low cell potential after the structural rearrangements occurring in the first cycle, that well matches with the experimental evidence of a potential plateau at about 2.7-2.8 V (vs. Li reference electrode) during the second and the subsequent cycles. This structure is particularly stable due to its large cation-cation spacing with minimal extra distortion into the tetrahedral sites [24-26] which accounts for the irreversible formation of the disordered *$Pmn2_1$* phase. All of these theoretical works underline the difficulty in extracting the second Li^+ due to the high electrochemical potential needed for the oxidation of Fe^{3+} to Fe^{4+}. The reported potential value for this oxidation ranges between 4.8 and 4.85 V vs. Li depending on the starting polymorph. Zhang et al. [27], proposed a diagram for the $P2_1/n$ polymorph of the possible charge-discharge mechanisms for a multi-electron process, trying to explain the differences of the second oxidation potential observed at about 4.3 or 4.8 V vs. Li and reported in other experimental works. This difference could depend on the structural

transformation, which, in turn, depends on many experimental conditions such as temperature, charge/discharge rate and particle size [27]. In particular, Zhang et al. [27] reported that, even if the charge compensation for the iron oxidation in $Li_{0.5}FeSiO_4$ could lead to oxidation of oxygen ions, actually the structure is stable and oxygen release is energetically unfavourable. The formation of this structure could explain the high specific capacity value of about 200 mAh g^{-1} demonstrated in some experimental works (see 2.2 paragraph). By the way, the second oxidation is accompanied by a relevant volume variation, thus negatively affecting the long-term cycling behaviour of the material [24]. Therefore, the structural instability due to the high electrochemical potential of the second oxidation hinders the possibility of extraction of a second lithium ion, thus unfortunately making the lithium metal orthosilicate a medium capacity material.

The Li^+ diffusion coefficient was calculated and very low values were reported, ranging between 10^{-10} and 10^{-14} cm^2 s^{-1} [28, 29], definitely lower than the low conducting $LiFePO_4$ (~ 10^{-7} cm^2 s^{-1}). A much more lower value of about 10^{-20} cm^2 s^{-1} was also found at room temperature [30], thus further suggesting that Li_2FeSiO_4 does not provide an improved kinetics compared to the state-of-the-art cathode materials. For what concerns the migration pathways of the lithium ions, it was found that, in case of the disordered *Pmn2₁* structure, the lithium migration barrier remains similar to that of the pristine structure. As a result, the exchange of Li/Fe on the cation sites does not negatively affect the electrochemical performance, notwithstanding the tortuosity of the migration pathways. Other works [26, 30] calculated the energy of lithium migration for the *P2₁* and *P2₁/n* structures, both for the pristine and the cycled material, taking into consideration different pathways. The accurate analysis of the results indicated that a zigzag trajectory in the *ac* plane is generally favoured, but also other paths show similar activation barriers, thus contributing to the overall 2-dimensional ionic diffusion [26,30].

2.2 - Experimental studies

2.2.1 - Conventional electrochemical studies

In 2005, Nyten et al. [31] reported the first electrochemical characterization in lithium cell of a Li_2FeSiO_4-based cathode. A *Pmn2₁* structure was assigned to the lithium iron orthosilicate on the basis of its isostructurality with Li_3PO_4 but, based on the following works, it seems more correct to consider the material as a *P2₁/n* polymorph. However, the electrochemical behaviour of the sample was clearly discussed based on the results of cyclic voltammetry and galvanostatic charge/discharge cycling tests (see Figure 3). The lowering of the potential plateau from 3.10 to 2.8 V vs. Li during the first cycle, suggested a phase transition to a more stable structure after the initial cycles; a promising capacity of about 165 mAh g^{-1} was obtained at 60 °C and C/16 current rate. In the

research articles published thereafter, most of the authors described a similar behaviour, ascribed to the structural rearrangements during the initial cycles [32-34]. Anyway, a noticeable variance may be found among the bibliographic reports regarding the values of potential where the iron oxidation reaction occurs [35-37], which is likely due to the different synthetic approaches adopted, resulting in materials having different particle size and carbon coating. Due to its capability of operating close to the equilibrium potential, the GITT technique was used to clarify the first oxidation potential of Li_2FeSiO_4, which was found to be different depending on the polymorph structure (i.e., 2.9 V for the *Pmnb*, 3.0 V for the $P2_1/n$ and 3.1 V vs. Li for the $Pmn2_1$) [38]. These different values were explained taking into account variations in the arrangements, orientation, size and distortion of the FeO_4 tetrahedra. The authors also discussed how the current density influences the kinetics of the thermodynamic stabilization process which, in turn, depends on the temperature at which the electrochemical test is performed [38]. Other authors performed GITT measurements highlighting a shift in the potential values between the oxidation and reduction reactions (i.e., from 3.1 to 2.7 V vs. Li, see Figure 4) [39]. Such a large overpotential, accounting for a high electrode polarization, is due to the low reaction kinetics typical of Li_2FeSiO_4 resulting from its low electronic and ionic conductivities.

Another interesting point, which still deserves to be clarified, is the possibility of oxidizing the Fe^{3+} atoms to Fe^{4+} thus resulting in the extraction of two Li^+ ions per formula unit, consequently achieving the full theoretical specific capacity of about 330 mAh g^{-1}. This redox process was theoretically estimated to occur at about 4.8 V vs. Li. Muraliganth et al. [32] effectively showed this oxidation to occur at 4.7 V vs. Li for a nanostructured sample obtained by microwave-solvothermal synthesis (monoclinic $P2_1$), as resulting from the charge/discharge profile obtained for a cell cycled at 55 °C and C/20 rate (Figure 5a and b). Other works described the same oxidation process occurring at about 4.3 V, based on the charge plateau and on the differential capacity curve (Figure 5c and d) [8,13,40]. Besides, other authors suggested the formation of Fe^{4+} directly from the high capacity value of 220 mAh g^{-1} achieved by the cell upon charge [41]. In order to demonstrate the presence of Fe^{4+} atoms, specific spectroscopic techniques such as Mössbauer and XAS/XANES, must be used to investigate the electrodes in their charged state. *Ex situ* Mössbauer measurements performed on electrodes charged to various potential values demonstrated the presence of Fe^{4+} ions, the amount of which increased from 20.7 to 58.2 % passing from 4.2 to 4.6 V vs. Li, respectively [13]. Similar results were observed by means of Mössbauer as well as *in situ* XAS experiments on a cell fully charged up to 4.8 V vs. Li [8, 42].

Several works dealt with the electrochemical performances of Li_2FeSiO_4 in terms of charge/discharge specific capacity and cycling stability. The initial studies reported rather low

specific capacities, far from the theoretical value, likely due to the very low electronic conductivity of the pristine material. Thus, many efforts were done to optimize some specific characteristics and properties of this material, such as the carbon coating on the particles, the addition of carbon nanotubes [40] or the elaboration of porous/nanocomposite cathodes [13,32-33,36,43] having fine-tuned morphologies [41, 44]. Some recent works demonstrated prolonged cycling (i.e., about 500 cycles) with a specific capacity around 150 [43] or 120 mAh g^{-1} [44] at current regimes as high as 1C or 5C, respectively (see Figure 6a). By increasing the current rate up to 20C, the specific capacity values decreased to about 100-80 mAh g^{-1} [43-44]. These good performances were reached thanks to the hierarchical porous structure of the composite Li_2FeSiO_4/C cathode prepared by an *in situ* templated method [43] or to nanoworm-like particles obtained by using a triblock copolymer structure directing agent [44].

The stability of Li_2FeSiO_4 upon aging and versus the conventional electrolytes is another important issue which deserves to be thoroughly investigated. At first, Nyten et al. [45] discussed the surface state of cathodes extracted from a cell assembled using as the electrolyte a 1.0 M solution of lithium bis(trifluoromethyl sulfonyl)imide (LiTFSI) in a 1:1 mixture of ethylene carbonate (EC) and propylene carbonate (PC). Small amounts of solvent reaction products, possibly Li carboxylates, were found on the cathode surface, but the main component of the surface film was LiTFSI salt in its original form. In a successive work, Ensling et al. [46] studied the Li_2FeSiO_4 stability in different electrolytes based on lithium hexafluorophosphate ($LiPF_6$) and LiTFSI salts. They concluded that the cathode was degraded by the HF formed by fluorinated electrolytes. More comprehensive and recent studies on the same topic [47-48] were carried out by aging Li_2FeSiO_4 powder for 40 days in different electrolytes at 20 and 60 °C. Relevant structural changes were detected for the powder aged at 60 °C in $LiPF_6$ and $LiBF_4$ based electrolytes: an important overall degradation of the pristine material was observed, resulting in the formation of lithium hexafluorosilicate (Li_2SiF_6) and other compounds [47]. It was also shown that the aging stability of Li_2FeSiO_4 depends upon the polymorph structure. In this respect, the *Pmnb* polymorph was found to be the most stable due to the strong Fe-O bonds and to the interconnectivity between the tetrahedra of FeO_4 and LiO_4 [48]. As a result of these studies, some concerns have arisen regarding the choice of the suitable electrolyte and the conditions at which the lithium cells based on Li_2FeSiO_4 cathodes should be preferably operated.

So far, very few data are available on the electrochemical characterization of the mixed $Li_2Fe_{0.5}Mn_{0.5}SiO_4$ compound. In general, the Mn substitution in the Li_2FeSiO_4 framework seems not to provide significant improvements in both capacity and cycling stability. The effect of Mn substitution on the cycling performance is shown in Figure 6(b,c) [15, 16]; in both cases a lower

discharge capacity was observed when the amount of Mn is increased to > 0.2 mol per formula unit. The analysis of the differential capacity curves provided information on the oxidation potentials of $Li_2Fe_{1-x}Mn_xSiO_4$; the increase with "x" in the potential values was ascribed to the combination of the electrochemical properties of Fe and Mn [16]. In addition, an indication of a higher electrochemical reversibility of samples with low amount of Mn substitution was reported.

2.2.2 - *In* and *ex* situ studies of Li_2FeSiO_4

An optimal experimental approach to study the modifications occurring on the materials during cycling is the combined use of *ex situ* and *in situ* diffraction/spectroscopic techniques (e.g., XRD, XAS, XANES, MAS-NMR and Mössbauer) and electrochemical measurements. In the recent years, plenty of works were published regarding *in situ* measurements, mainly exploiting the great potential and capability offered by Synchrotron and Neutron facilities where the high energy beam enables to obtain high resolution data. However, different results regarding lithium metal orthosilicates were published so far, often showing measurements performed in very different experimental conditions e.g., potential window, current rate, electrolytes, temperature and number of cycles) as shown in Table 1. Therefore, every single case will be thoroughly discussed in the followings.

In 2006, the first research article was published on an *in situ* Synchrotron XRD analysis of a Li_2FeSiO_4/lithium cell after two complete cycles (see Table 1) [49]. *In situ* patterns were collected at the beginning of the cycling test and at the maximum potential values based on the corresponding CV plot. ^{57}Fe Mössbauer spectra evidenced a Fe^{2+}/Fe^{3+} conversion of 90 %, corresponding to the extraction of one Li^+ ion per mol. On the other hand, a value of 0.75 Li^+ was obtained by the analysis of the charge-discharge cycling results, which indicates that the impurity phases formed during synthesis contributed to the electrochemical process. Changes observed in the XRD patterns of the initial $Pmn2_1$ structure were attributed to a structural disorder of the $LiFeSiO_4$ charged phase due to exchange of Li and Fe ions. No structural transitions were evidenced and the $Pmn2_1$ disordered structure was maintained at the end of discharge. By means of *in situ* laboratory XRD, Dominko [21] showed a superior structural stability of Li_2FeSiO_4 with respect to the Li_2MnSiO_4 during cycling (see Table 1 for the experimental details); in agreement with the results from Nyten et al. [49] no structural transitions were evidenced. The Li_2FeSiO_4 sample could deliver a capacity of about 120 mAh g^{-1} (about 0.7 mol of Li) at C/20 and 100 mAh g^{-1} at C/2. It was suggested a two phase electrochemical oxidation/reduction process for Li_2FeSiO_4. By using *in situ* XAS and Mössbauer spectroscopy, the same author confirmed the structural stability of Li_2FeSiO_4 during cycling, finding that the local symmetry of Fe cations was practically unchanged. In addition, Fe^{4+}

ions were not evidenced in the charged sample, but the reason for such a behaviour was not clarified [10].

The observation of anti-site defect formation for the initial *P2₁/n* polymorph was reported by Kojima et al. [50], who discussed *ex situ* Synchrotron XRD results (Figure 7a). Patterns were collected after cell disassembly on a cathode charged and discharged at various states, i.e. charged up to 3.1 and 4.2 V vs. Li, discharged at 1.5 V and successively charged again at 4.2 V vs. Li (see Table 1). After the second cycle, a capacity of about 160 mAh g^{-1} was obtained, corresponding to one mol of lithium per formula unit. By means of Rietveld refinement, the authors demonstrated the formation of the anti-site defect (up to 50 % of Li/Fe exchange) which is irreversible during discharge, as also shown in ref. [49] for the *Pmn2₁* polymorph. Starting from the same *P2₁/n* structure, other authors claimed for completely different results. By *ex situ* XRD on a cathode operated for ten cycles in lithium cell, Armstrong et al. [18] observed a structural transition from *P2₁/n* to an inverse β_{II} *Pmn2₁* polymorph, the structure of which being similar to that of Li_2CoSiO_4. The sample delivered about 120 mAh g^{-1}, that is 0.7 Li^+ ions per mol extracted/inserted. Some similarities may be observed from the patterns of the disordered phase in the charged state reported by Kojima et al. [50] as well as from those of the inverse β_{II} polymorph (Figure 7b). On the other hand, having a site shared by Li and Fe, the inverse β_{II} phase is inherently disordered. Despite previous reports showed significant changes in the XRD patterns already during the first charge, in Armstrong's study some changes could be observed only after 5 cycles. The authors suggested that, in order to avoid structural modifications upon cycling, it could be useful to directly synthesise the inverse β_{II} polymorph, ready to be used as cathode in lithium cell [18].

A research article was recently published reporting an *in situ* laboratory XRD study [39] performed on a cell cycled under chronocoulometric mode. The collection of each XRD pattern lasted 6.9 hours and, at the end of charge, overall 0.85 Li^+ ions per mol were extracted. The pristine sample showed quite an important amount of impurities, such as Li_2SiO_3 and $LiFeO_2$, the diffraction peaks of which disappeared in the analysis of the cathode after discharge. In agreement with ref. [18], the authors claimed for a phase transition from the *P2₁/n* to the *Pmn2₁* structure; nevertheless, their experimental patterns looked appreciably different from those shown in the reference work [18]. The phase transition was found to be irreversible even in this case, and some peaks remained unidentified in the pattern of the discharged sample. A recent combined theoretical/experimental *in situ* Synchrotron XRD/XANES [51] study revealed the formation of the anti-site defect in the *P2₁/n* polymorph. The initial charge and discharge capacities were 280 and 190 mAh g^{-1} respectively, indicating the reversible extraction/insertion of more than one Li^+ ion; this was confirmed by XANES spectra demonstrating the formation of Fe^{4+} ions. Galvanostatic cycling was stopped at

fixed potentials and XRD patterns were collected after allowing the cell to rest for 30 min (see Figure 7c). A two phase transformation process was observed in the potential range below 4.1 V vs. Li, due to the extraction of one Li^+, as for the reaction:

$$Li_2FeSiO_4 \rightarrow LiFeSiO_4 + Li^+ + e^-$$

On the other hand, another phase transformation occurred in the high potential range between 4.1 and 4.8 V vs. Li, leading to the formation of the γ disordered Li_yFeSiO_4 ($0 < y < 1$) phase. The quality of the experimental XRD patterns was not sufficient for the Rietveld refinement. Therefore, to support and confirm the experimental evidences, DFT calculation was performed starting from the monoclinic $P2_1/n$ symmetry and simulating the XRD pattern by supposing site exchange of one half of the whole amount of Li^+ ions with all the iron ions (Figure 7d). As previously discussed, the disordered $P2_1/n$ structure was observed also by Kojima et al. [50], in a low potential range (i.e., 3.1-4.2 V vs. Li) where only the $LiFeSiO_4$ phase might be formed.

A very recent work [52] showed how the current rate could influence the phase transformation of Li_2FeSiO_4 during cycling (see Table 1 for experimental details). Starting from a $P2_1/n$ polymorph, the authors demonstrated the formation of the orthorhombic *Pmnb* polymorph at C/50 rate, while at C/10 the initial structure was maintained. This behaviour was explained suggesting the *Pmnb* structure as being the thermodynamically favourable phase that can be stabilized allowing sufficient time for the structural rearrangement.

Based on the above discussed findings, a clear contradiction in the results is still present so far, for which either polymorphic transitions or formation of defective structures appear equally plausible hypotheses. Therefore, we investigated the structural variations of the lithium metal orthosilicate system, trying to shed light on the behaviour of the cycled cathode material. The iron-based Li_2FeSiO_4 (hereafter named LFS) and the mixed $Li_2Fe_{0.5}Mn_{0.5}SiO_4$ (LFMS) structures were both synthesized by means of a sol-gel approach, in order to study their electrochemical behaviour during charge/discharge cycling in lithium cell by means of *in situ* Synchrotron XRD measurements. Synthesis conditions, electrode preparation procedures and cell assembly for the *in situ* XRD diffraction measurements are described in Table 2 and in refs. [7,17,53]. The comparison between the synchrotron patterns of the two pristine powders before *in situ* analysis is shown in Figure 8a. A different polymorph structure is revealed for the LFS series of samples with respect to the LFMS one; clearly, in this latter case the peak at about 5.36° is not observable and the peak at about 8.1° is shifted towards a lower angle (see the inset in Figure 8a). A broad peak typical of amorphous phases is present in the LFS-P sample, likely due to residual carbon traces. In addition, this sample shows broader peaks than LFS and LFMS, due to the effect of carbon in inhibiting the particle growth. The Rietveld refinement confirmed the structural differences among the samples.

In particular, the *P2$_1$/n s.g. (space group)* was assigned to LFS and LFS-P samples, while a mixture of *Pmnb* (main phase) and of *P2$_1$/n* (26 wt.%) polymorphs was observed in the LFMS one. In all the samples, traces (less than 10 %) of impurity phases (i.e., Li_2SiO_3, Fe and Fe_2SiO_4) were detected. In Figure 8a, a SEM micrograph of the LFS sample is also shown as inset; it is representative for all the prepared samples which show similar morphologies having rounded particles typical of sol-gel synthesis.

The *in situ* XRD measurements were performed using a lithium test cell assembled in a "coffee bag" envelope [53] and suitably modified by the addition of a Kapton® window in order to perform measurements in transmission mode (see Figure 8b). The experimental conditions used for galvanostatic cycling are reported in Table 1. The *in situ* study was performed in the range between –5° and 17° 2θ degrees at a speed of 3 degrees per minute corresponding to about 7 minutes for each measurement, without any pause between one pattern and the following, during continuous cell cycling. This means a remarkable number of patterns collected for each charge/discharge cycle, where each pattern recorded represents a snapshot of the cathode structure at the corresponding potential value. Our LFS cathode delivered about 100 and 140 mAh g^{-1} for the first and the second charge step, respectively, thus showing performances comparable to those reported in the literature and previously discussed. The comparison between the patterns of sample LFS, collected during the two initial charge cycles, is shown in Figure 9. An evident decrease in the intensity of all the reflections of the pristine Li_2FeSiO_4 can be observed together with a different intensity ratio between the peaks. In particular, the peaks in the 5-6/2θ range retain their intensity, which suggests an increase in the disorder degree during the second cycle. No structural transitions are detectable.

The series of results for our LFS-P sample is reported in Figure 10. This sample showed a high degree of disorder of the *P2$_1$/n* crystal structure before the charge/discharge measurements. Before the *in situ* analysis, it was studied by cyclic voltammetry. The resulting plot is shown in Figure 10a. During the first cycle, the Fe oxidation peak is clearly observed at about 2.9 V vs. Li, that remains unmodified during the second cycle. A slight shift towards lower values is observed during the third cycle; successively, the profile remains almost unchanged. The low potential of 2.9 V vs. Li we obtained, which is lower than the 3.1 V usually reported during the first cycle, could indicate that the sample is in the disordered form, at least partially, already before cycling. This evidence is in good agreement with the observations from other authors who reported a shift towards lower potential values for the disordered structure obtained upon cycling [31]. This may suggest that our sample contains a significant amount of an inverse $LiFeSiO_4$ structure before cycling. The disordered LFS-P sample (Figure 10d) was obtained by ball milling the pristine powder that, as shown in Figure 8a, had a *P2$_1$/n* crystal structure without any evidence of disorder. Then, a half cell

was prepared for *in situ* measurement and this cell was charged/discharged for 4 cycles before analysis, obtaining a charge capacity of about 125 mAh g^{-1} during the first charge (see Figure 10b). These electrochemical measurements were done in order to better investigate the effect of galvanostatic cycling on the orthosilicate structure, but also to put into evidence the differences with respect to an ordered crystal structure. Our investigation follows the comment by Armstrong et. al [18] on the opportunity of directly synthesizing the disordered structure, thus avoiding the structural changes occurring upon cycling. None of the main characteristics peaks of Li_2FeSiO_4 can be observed in the *in situ* synchrotron patterns of the charged/discharged cathode, while the peaks related to the disordered phase are visible (peaks circled in Figure 10c). The same reflections (peaks circled in Figure 10d) are detected both on the as prepared cathode and on the ball milled cathode powder, which clearly demonstrates that no further modification occurs upon cycling (see the *ex situ* pattern of Figure 10d). Apparently, neither shifts in the peak positions nor polymorphic transitions are evident, thus suggesting a high structural stability of the monoclinic $P2_1/n$ disordered phase, in agreement with the theoretical calculations [27] as well as with the findings by Kojima et al. [50].

The disordered polymorph appeared to be air-sensitive since the formation of Li_2CO_3 was detected after *ex situ* XRD analysis of the cathode stored for few hours under ambient atmosphere (see Figure 10d). The instability of the inverse β_{II} polymorph upon exposure to air, that could lead to the formation of Li_2O or Li_2CO_3, was theoretically proposed by Seo and co-workers [26] and is here definitively confirmed by our experimental results.

2.2.3 - *In situ* and *ex situ* studies of $Li_2Fe_{0.5}Mn_{0.5}SiO_4$

At present, very few information is available regarding *in situ* studies on the mixed $Li_2Fe_{1-x}Mn_xSiO_4$ cathode material, even though it has very interesting prospects because the presence of Mn could assure a better structural stability [21]. Mixed compositions such as $Li_2Fe_{0.75}Mn_{0.25}SiO_4$ [21] and $Li_2Fe_{0.8}Mn_{0.2}SiO_4$ [42] were studied by *in situ* and *ex situ* XRD and *in situ* XAS. While Dominko [21] showed a good structural stability up to 4.2 V vs. Li, Chen et al. [42] suggested a structural transition from $P2_1/n$ to $Pmn2_1$ s.g. after cycling up to 4.8 V (see Table 1) in agreement with Armstrong et al. [18].

The mixed $Li_2Fe_{0.5}Mn_{0.5}SiO_4$ orthosilicate was synthesized, and analysed in the present work. It showed the presence of the *Pmnb* polymorph along with about 26 % of the $P2_1/n$ phase. The formation of a mixture of polymorphs is not unusual for this composition and was observed by other authors as well [4]. The results of the *in situ* XRD study are shown in Figure 11a. The pristine sample shows a high crystalline degree, which is well maintained during charge up to 4.5 V vs. Li

at C/20 rate (obtained capacity of about 180 mAh g^{-1}, see Figure 11b). The lattice parameters remain practically unchanged: *Pmnb* phase with a = 6.2747(28), b= 10.7158(47), c = 5.0004(21) Å at OCV, and a = 6.2705(40), b = 10.7239(65), c = 4.9997(30) Å at 4.5 V vs. Li. It is evident that no anti-site defect is present as confirmed by an *ex situ* XRD pattern collected on the disassembled cathode material. These results are in good agreement with those shown by Dominko et al. [21]; thus, we can here confirm the stabilizing effect of the Mn ions that, differently from what observed for the Li_2FeSiO_4 compound, may inhibit structural transitions in the mixed orthosilicate.

3- Chemically delithiated Li_2FeSiO_4

A different approach to study the delithiated phases and to clarify the mechanism of Li insertion/extraction was the preparation of the chemically delithiated Li_2FeSiO_4 [19,54]. In ref. [54], the pristine Li_2FeSiO_4 sample was shown to have the *Pmnb* crystal structure. Samples with Li^+ content up to 0.12 (i.e., $Li_{0.12}FeSiO_4$) were prepared and, upon XRD analysis, a continuous amorphization was observed while increasing the degree of delithiation [54]. An initial evidence of disorder can be observed for the $Li_{1.54}FeSiO_4$ sample due to the increased intensity of the diffraction peaks in the range of 20-25°/2θ. These observations were supported by HRTEM analysis coupled with electron diffraction SAED. The authors did not show results for a $LiFeSiO_4$ sample, thus it cannot be directly compared with *in situ* measurements, where this phase is often shown. XANES spectra were also recorded to study the iron oxidation state in the delithiated phases and the authors demonstrated that no Fe^{4+} ions formation occurred even in the fully delithiated sample.

Starting from the $P2_1/n$ polymorph, Lee et al. [19] showed that the crystal structure is stable up to the extraction of 0.66 Li^+. By using Mössbauer spectroscopy, the authors identified the coexistence of Fe^{2+}/Fe^{3+} valence states in the delithiated $Li_{2-x}FeSiO_4$ compound. A $Li_{1.34}FeSiO_4$ sample was rather comparable with the $Li_{1.3}FeSiO_4$ obtained by electrochemical delithiation and discussed in the previous section [18, 21], but for the chemically delithiated sample neither phase transitions nor anti site defect were clearly evidenced.

For clarity purposes, we must conclude that the direct comparison between the results obtained by analysing samples delithiated by chemical or electrochemical methods may be not truly consistent because of the different ways Fe^{2+} is oxidised.

4– Concluding remarks

In the present perspective, an attempt has been made to comprehensively review the structure-dependent electrochemical characteristics of the lithium metal orthosilicate family of compounds,

taking into consideration the main consolidated as well as the still existing issues based on the most recent and significant literature reports. At present, both structural and spectroscopic properties are well defined for the pristine material. On the contrary, when the structural variations occurring during lithium extraction/insertion upon cycling are particularly considered, several aspects need to be clarified. Based on the results herein discussed, the amorphization of Li_2FeSiO_4 during cycling can be excluded, while the formation of a disordered phase has been observed by almost all the authors. The crystal structure of the disordered phase seems to vary from an inverse β_{II} *Pmn2₁* phase to an inverse monoclinic *P2₁/n*. Understanding the mechanism for the preferential formation of one or the other of these two structures is not at all trivial; in fact, many factors could be responsible for such a behaviour, including the kind of pristine structure, the presence of relevant amount of Fe^{3+} in the pristine material, the microstructural characteristics, the presence and amount of carbon coating as well as other experimental conditions.

Another important challenge is the formation of Fe^{4+} combined with the extraction of two Li^+ ions per formula unit, thus resulting in the delivery of the full theoretical capacity. Nevertheless, kinetic and thermodynamic properties could represent a limitation to the complete iron oxidation.

It has been shown that aging can be responsible for the cathode material degradation, which results in the formation of different phases depending on the electrolyte, the contact with ambient air and/or the operating temperature. The investigation of the reactivity of the orthosilicate active material in contact with the electrolyte is likely to be fundamental, most importantly if one considers that the second oxidation step occurs at potential values exceeding 4.5 V versus the lithium metal reference electrode.

For what concerns the mixed $Li_2Fe_{0.5}Mn_{0.5}SiO_4$ compound, neither amorphization nor structural transition have been observed so far, even upon cycling, which suggests a noticeable structural stability. This compound can be obtained having an orthorhombic *Pmnb* structure as the main phase and the superior stability of this structure was discussed also during aging studies.

It can be concluded that, at present, Li_2FeSiO_4 could represent a cathode material having limited capacity and cyclability: many efforts should be devoted to the optimization of those properties accounting for Li^+ ions diffusion and specific conductivity.

Acknowledgments

We acknowledge the European Synchrotron Radiation Facility for provision of synchrotron radiation facilities and we would like to thank Dr. Andy Fitch for assistance in using beamline ID31 during experiment MA1757. This work was performed in the frame of Cariplo Project 2011-0325 “New electrolyte and electrode materials for thin-film lithium microbatteries”.

References

1. Z. Gong and Y. Yang, *Energy Environ. Sci.*, 2011, **4**, 3223-3242.
2. M. S. Islam, R. Dominko, C. Masquelier, C. Sirisopanaporn, A.R. Armstrong and P.G. Bruce, *J. Mater Chem.*, 2011, **21**, 9811-9818.
3. S. Nishimura, S. Hayase, R. Kanno, M. Yashima, N. Nakayama and A. Yamada, *J. Am. Chem. Soc.,* 2008, **130**, 13212–13213.
4. C. Sirisopanaporn, R. Dominko, C. Masquelier, A. R. Armstrong, G. Mali and P. G. Bruce, *J. Mater. Chem.*, 2011, **21**, 17823-17831.
5. G Mali, M. Rangus, C. Sirisopanaporn and R. Dominko, *Solid State Nuclear Magnetic Resonance,* 2012*,* **42**, 33-41.
6. G. Mali, C. Sirisopanaporn, C. Masquelier, D. Hanzel and R. Dominko, *Chem. Mater.*, 2011, **23**, 2735-2744.
7. M. Bini, S. Ferrari, C. Ferrara, M. C. Mozzati, D. Capsoni, A. J. Pell, G. Pintacuda, P. Canton and P. Mustarelli, *Scientific Reports*, 2013, **3**, 3452.
8. X. Wu, X. Jiang, Q. Huo and Y. Zhang, *Electrochimica Acta,* 2012, **80**, 50-55.
9. D. Lv, J. Bai, P. Zhang, S. Wu, Y. Li, W. Wen, Z. Jiang, J. Mi, Z. Zhu and Y. Yang, *Chem. Mater,* 2013, **25**, 2014-2020.
10. R. Dominko, I. Arcon, A. Kodre, D. Hanzel and M. Gaberscek, *J. Power Sources*, 2009, **189**, 51-58.
11. C. Sirisopanaporn, A. Boulineau, D. Hanzel, R. Dominko, B. Budic, A. R. Armstrong, P. G. Bruce and C. Masquelier, *Inorg. Chem.*, 2010, **49**, 7446-7451.
12. C. Boulineau, R. Sirisopanaporn, R. Dominko, A. R. Armstrong, P. G. Bruce and C. Masquelier, *Dalton Trans.*, 2010, **39**, 6310-6316.
13. D. Lv, W. Wen, X. Huang, J. Bai, J. Mi, S. Wu and Y. Yang, *J. Mater. Chem.*, 2011, **21**, 9506-9512.
14. Z. L. Gong, Y. X. Li and Y. Yang, *Electrochem. Solid-State Letters*, 2006, **9**, A542-A544.
15. B. Shao, Y. Abe and I. Taniguchi, *Powder Tech.*, 2013, **235**, 1-8.
16. C. Deng, S. Zhang, S and Y. Yang, *J. Alloys Compounds*, 2009, **487**, L18-L23.
17. M. Bini, S. Ferrari, D. Capsoni, C. Spreafico, C. Tealdi and P. Mustarelli, *J. Solid State Chem.,* 2013, **200**, 70−75.
18. A. R. Armstrong, N. Kuganathan, M. S. Islam and P. G. Bruce, *J. Am. Chem. Soc.*, 2011, **133**, 13031-13035.
19. I. K. Lee, S. J. Kim, T. Kouh and C. S. Kim, *J. Appl. Phys.*, 2013, **113**, 17E306-1.

20. K. Zaghib, A. Ait Salah, N. Ravet, A. Mauger, F. Gendron and C.M. Julien, *J. Power Sources*, 2006, **160**, 1381–1386.
21. R. Dominko, *J. Power Sources*, 2008, **184**, 462-468.
22. R. Dominko, M. Bele, A. Kokalj, M. Gaberscek and J. Jamnik, *J. Power Sources*, 2007, **174**, 457-461.
23. A. Kokalj, R. Dominko, G. Mali, A. Meden, M. Gaberscek and J. Jamnik, *Chem Mater.*, 2007, **19**, 3633-3640.
24. A. Saracibar, A. Van Der Ven and M. E. Arrojo-de Dompablo, *Chem. Mater.*, 2012, **24**, 495-503.
25. C. Eames, A. R. Armstrong, P. G. Bruce and M. S. Islam, *Chem. Mater.*, 2012, **24**, 2155-2161.
26. D. H. Seo, H. Kim, I. Park, J. Hong and K. Kang, *Phys. Rev. B*, 2011, **84**, 220106.
27. P. Zhang, Y. Zheng, S. Yu, S. Q. Wu, Y. H. Wen, Z. Z. Zhu and Y. Yang, *Electrochimica Acta*, 2013, **111**, 172-178.
28. A. Liivat and J. O. Thomas, *Solid State Ionics*, 2011, **192**, 58–64.
29. D. Su, H. Ahn and G. Wang, *Appl. Phys. Let.*, 2011, **99**, 141909.
30. R. B. Araujo, R. H. Scheicher, J. S. de Almeida, A. Ferreira da Silva and R. Ahuja, *Solid State Ionics*, 2013, **247-248**, 8-14.
31. A. Nyten, A. Abouimrane, M. Armand, T. Gustafsson and J. O. Thomas, *Electrochem. Comm.,* 2005, **7**, 156-160.
32. T. Muraliganth, K. R. Stroukoff and A. Manthiram, *Chem. Mater.*, 2010, **22**, 5754-5761.
33. Z. L. Gong, Y. X. Li, G. N. He, J. Li and Y. Yang, *Electrochem. Solid State Lett.*, 2008, **11**, A60-A63.
34. N. Yabuuchi, Y. Yamakawa, K. Yoshii and S. Komaba, *Dalton Transaction*, 2011, **40**, 1846-1848.
35. R. Dominko, D. E. Conte, D. Hanzel, M. Gaberscek and J. Jamnik, *J. Power Sources*, 2008, **178**, 842-847.
36. Z. Zheng, Y. Wang, A. Zhang, F. Cheng, Z. Tao and J. Chen, *J. Power Sources*, 2012, **198**, 229-235.
37. L. Hong and Z. Zhang, *Russian J. Electrochem.*, 2013, **49**, 386-390.
38. C. Sirisopanaporn, C. Masquelier, P. G. Bruce, A. R. Armstrong and R. Dominko, *J. Am. Chem. Soc.*, 2011, **133**, 1263-1265.
39. H. Zhou, M. A. Einarsrud and F. Vullum-Bruer, *J. Power Sources*, 2013, **238**, 478-484.

40. Y. Zhao, J. Li, N. Wang, C. Wu, Y. Ding and L. Guan, *J. Mater. Chem*., 2012, **22**, 18797-18800.
41. D. Rangappa, K. D. Murukanahally, T. Tomai, A. Unemoto and I. Honma, *Nano Lett.*, 2012, **12**, 1146-1151.
42. R. Chen, R. Heinzmann, S. Mangold, V. S. Kiran Chakravadhanula, H. Hahn and S. Indris, *J. Phys. Chem. C*, 2013, **117**, 884-893.
43. Z. Chen, S. Qiu, Y. Cao, J. Qian, X. Ai, K. Xie, X. Hong and H. Yang, *J. Mater. Chem. A*, 2013, **1**, 4988-4992.
44. X. Wu, X. Wang and Y. Zhang, *ACS Appl. Mat. Interf.*, 2013, **5**, 2510-2516.
45. A. Nyten, M. Stjerndahl, H. Rensmo, H. Siegbahn, M. Armand, T. Gustafsson, K. Edstrom and J. O. Thomas, *J. Mater. Chem.*, 2006, **16**, 3483-3488.
46. D. Ensling, M. Stjerndahl, A. Nyten, T. Gustafsson and John O. Thomas, *J. Mater. Chem.*, 2009, **19**, 82-88.
47. C. Dippel, S. Krueger, R. Kloepsch, P. Niehoff, B. Hoffmann, S. Nowak, S. Passerini, M. Winter and J. Li, *Electrochimica Acta*, 2012, **85**, 66-71.
48. C. Dippel, S. Krueger, V. Kraft, S. Nowak, M. Winter and J. Li, *Electrochimica Acta*, 2013, **105**, 542-546.
49. A. Nyten, S. Kamali, L. Haggstrom, T. Gustafsson and J. O. Thomas, *J. Mater. Chem.*, 2006, **16**, 2266-2272.
50. A. Kojima, T. Kojima and T. Sakai, *J. Electrochem. Soc.*, 2012, **159**, A525-A531.
51. D. Lv, J. Bai, P. Zhang, S. Wu, Y. Li, W. Wen, Z. Jiang, J. Mi, Z. Zhu and Y. Yang, *Chem. Mater.*, 2013, **25**, 2014-2020.
52. T. Masese, Y. Orikasa, Cédric Tassel, J. Kim, T. Minato, H. Arai, T. Mori, K. Yamamoto, Y. Kobayashi, H. Kageyama, Z. Ogumi, and Y. Uchimoto, *Chem. Mater.*, 2014, **26**, 1380-1384.
53. J.R. Nair, M. Destro, C. Gerbaldi, R. Bongiovanni, N. Penazzi, *J. Appl. Electrochem.,* 2013, **43**, 137-145.
54. O. Kamon-In, W. Klysubun, W. Limphirat, S. Srilomsak, N. Meethong, *Physica B*, 2013, **416**, 69-75.

Tables

Table 1 – Experimental set-up for the cycling of Li_2FeSiO_4 and $Li_2Fe_{0.5}Mn_{0.5}SiO_4$ cathodes for *in* and *ex situ* XRD measurements.

Temperature	Current rate and number of cycles	Potential window	Electrolyte	λ (Å)	Ref.	Initial crystal structure	Final crystal structure
60°C	C/25 2 cycles	2.0-3.7 V	1M LiTFSI EC:PC 1:1	1.2519 *in situ*	49	$Pmn2_1$	$Pmn2_1$ with anti-site
60°C	C/50 -	2.0-4.1 V	LiBOB EC:DEC 1:1	Cukα *in situ*	21	not declared	The structure is maintained
60°C	C/15 2 cycles	1.5-4.2 V	1M $LiPF_6$ EC:DEC 1:1	0.7 *ex situ*	50	$P2_1/n$	$P2_1/n$ with anti-site
50°C	C/16 10 cycles	2.0-3.7 V	1M LiTFSI EC:DEC 1:1	Fekα *ex situ*	18	$P2_1/n$	β_{II} $Pmn2_1$
a. t.	– 1 cycle	2.85-3.25 V	1M $LiPF_6$ EC:DEC 3:7	Cukα *in situ*	39	$P2_1/n$	$Pmn2_1$
a. t.	10 mAg^{-1} charge 20 mAg^{-1} discharge 1 cycle	1.5-4.8 V	1M $LiPF_6$ EC:DEC 1:1	1.2398 *in situ*	51	$P2_1/n$	$P2_1/n$ with anti-site (γ $P2_1/n$)
a. t.	C/10 C/50 1 cycle	1.5-4.5V	1M $LiPF_6$ EC:DMC 1:1	0.49995 *ex situ*	52	$P2_1/n$	Pmnb or $P2_1/n$
a. t.	C/20	2.0-4.5 V	1M $LiClO_4$ EC:DEC 1:1	0.3999 *in situ*	this paper	see Table2	see 2.2.2 section
a. t.	C/40 1 cycle	1.5-4.8 V	1M $LiPF_6$ EC:DMC 1:1	Cukα *ex situ*	42	$P2_1/n$	β_{II} $Pmn2_1$

Table 2 – Acronym, synthesis condition, crystal structure of the samples and electrode composition.

Sample	**Reagents**	**Thermal treatment**	**Initial crystal structure**	**Electrode composition**
LFS	$FeC_2O_4 \cdot 2H_2O$ $LiCOOCH_3 \cdot 2H_2O$ TEOS, ethanol (see ref. 7)	10h 700°C in Ar	$P2_1/n$	70:20:10 LFS:AB:PVDF
LFS-P	$Fe(NO_3)_3 \cdot 9H_2O$ $LiNO_3$ TEOS, water and ethanol Pluronic (see ref. 44)	10h 700°C in Ar	$P2_1/n$	70:20:10 LFS-P:AB:PVDF
LFMS	$FeC_2O_4 \cdot 2H_2O$ $Mn(CH_3COO)_2 \cdot 4H_2O$ $LiCOOCH_3 \cdot 2H_2O$ TEOS, ethanol (see ref. 17)	10h 700°C in Ar	*Pmnb* and $P2_1/n$	70:20:10 LFMS:AB:PVDF

Figure Captions

Figure 1- Structure of the Li_2FeSiO_4 polymorphs a) *$P2_1/n$*, b) *Pmnb*, c) *$Pmn2_1$*, and d) inverse *$Pmn2_1$* (β_{II}) (reprinted with permission of ACS ref. [25]).

Figure 2- Calculated total energy difference of $Li_{2x}FeSiO_4$ polymorphs: a) Li_2FeSiO_4, b) $LiFeSiO_4$ and c) $FeSiO_4$. Other known structures are labelled in blue (reprinted with permission of ACS ref. [24]).

Figure 3- a) Cyclic voltammetry of Li_2FeSiO_4 at 80 °C and 20 mV h^{-1} and b) charge/discharge profile at 60 °C and C/16 (reprinted with permission of Elsevier ref. [31]).

Figure 4- Galvanostatic intermittent titration technique (GITT) profile for the initial charge and discharge of a nanoporous Li_2FeSiO_4/C cathode. Dashed lines are the corresponding coulometric titration curves derived from the GITT profiles (reprinted with permission of Elsevier ref. [39]).

Figure 5- a) Charge/discharge profiles recorded at C/20 rate and 55 °C, b) dQ/dV vs. potential plots of Li_2FeSiO_4/C (reprinted with permission of ACS ref. [32]), c) typical charge/discharge curves, d) dQ/dV vs. potential plot (30^{th} charge curve) of the MWNT@Li_2FeSiO_4 composite at a current density of 1C between 1.5 V and 4.7 V vs. Li (reprinted with permission of RSC ref. [40]).

Figure 6- a) Cycling behaviour of the Li_2FeSiO_4–C composite nanoworms and nanoparticles at high current rates (reprinted with permission of ACS ref. [44]), b) cyclability at 1C rate of the $Li_2Fe_xMn_{1-x}SiO_4$/C nanocomposites for x = 0, 0.2, 0.5 and 0.8 (reprinted with permission of Elsevier ref. [15]), c) cycling performance of the $Li_2Fe_{1-x}Mn_xSiO_4$ samples (reprinted with permission of Elsevier ref. [16]).

Figure 7- a) XRD patterns of the Li_2FeSiO_4 at various states of charge/discharge (reprinted with permission of ECS ref. [50]), b) fitted powder diffraction patterns for the Li_2FeSiO_4 electrode analysed at the end of the 10^{th} discharge cycle (reprinted with permission of ACS ref. [18]), c) *in situ* XRD patterns of the Li_2FeSiO_4 electrode at different preset voltages during charging process, d) computational XRD patterns of pristine Li_2FeSiO_4 (α), charged $LiFeSiO_4$ (β), and $Li_{0.5}FeSiO_4$ (γ) (reprinted with permission of ACS ref. [51]).

Figure 8- a) Synchrotron patterns of LFS, LFS-P and LFMS pristine powders (λ = 0.3999 Å) mounted in a 0.5 mm Lindemann capillary and measured in Debye–Scherrer (transmission) geometry (in the inset: enlarged view of the peak at about 8.1°/2θ and SEM micrograph of the LFS sample), b) photograph and scheme of the pouch cell used for *in situ* XRD. The house-made spectro-electrochemical cell assembly (configuration: working electrode, a fresh glass wool separator soaked into a 1.0 M $LiClO_4$ in a 1:1 EC:DEC liquid electrolyte and a lithium metal anode) was housed in a "coffee-bag" envelope hermetically sealed under vacuum in dry room. A belt of aluminium grid and a belt of copper grid were used as current collectors, for the cathode and the anode respectively. Before assembly, a hole (0.8 cm in diameter) was made in each side of the "coffee-bag" envelop, then sealed by a Kapton® sheet and faced with the electrode, in order to have a suitable "window" to perform the *in situ* X-ray diffraction measurements in transmission mode *in situ* during electrochemical cell cycling.

Figure 9- *In situ* Synchrotron patterns collected during the first and the second charge of our LFS sample.

Figure 10- a) Cyclic voltammetry at 0.1 mV sec^{-1} in the potential range between 2.5 and 4.5 V vs. Li, b) cycling behaviour before *in situ* XRD, c) *in situ* Synchrotron patterns of sample LFS-P during charge/discharge cycling at C/20 rate in the 2.0-4.5 V vs. Li potential range, d) in house XRD pattern of the pristine, *ex situ* and aged LFS-P cathode after 10 charge/discharge cycles. The asterisk "*" indicates Al, while "^" indicates Li_2CO_3 reflections.

Figure 11- a) *In situ* Synchrotron patterns during charge at C/20 in the 2.0-4.5 V vs. Li potential range and b) charge profile of the LFMS sample.

Figures

Figure 1

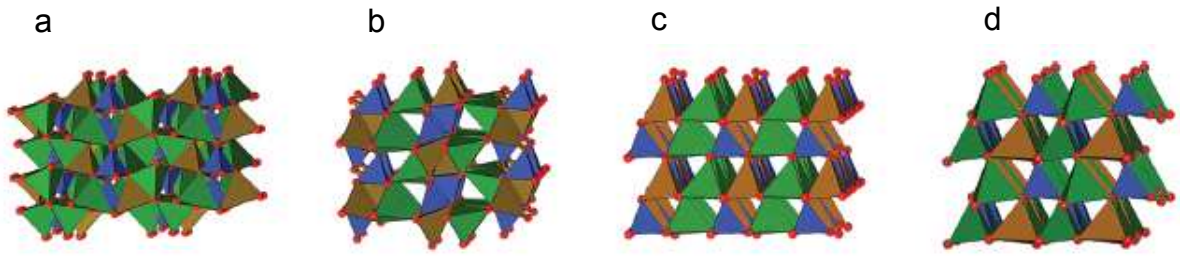

Figure 2

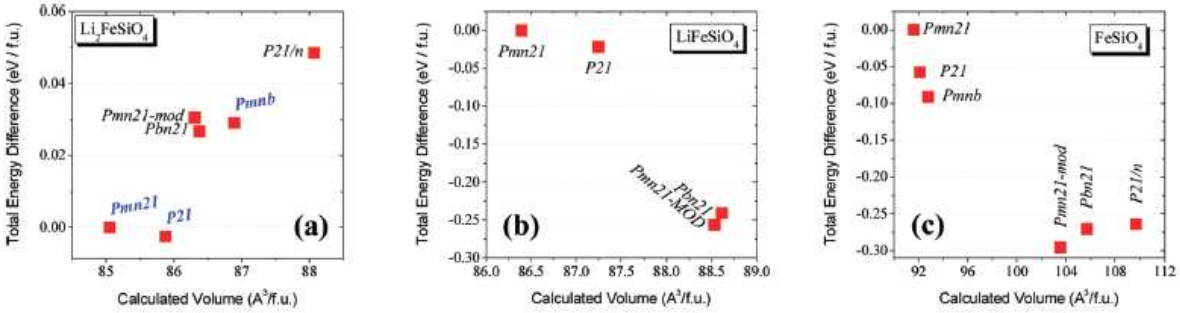

Figure 3

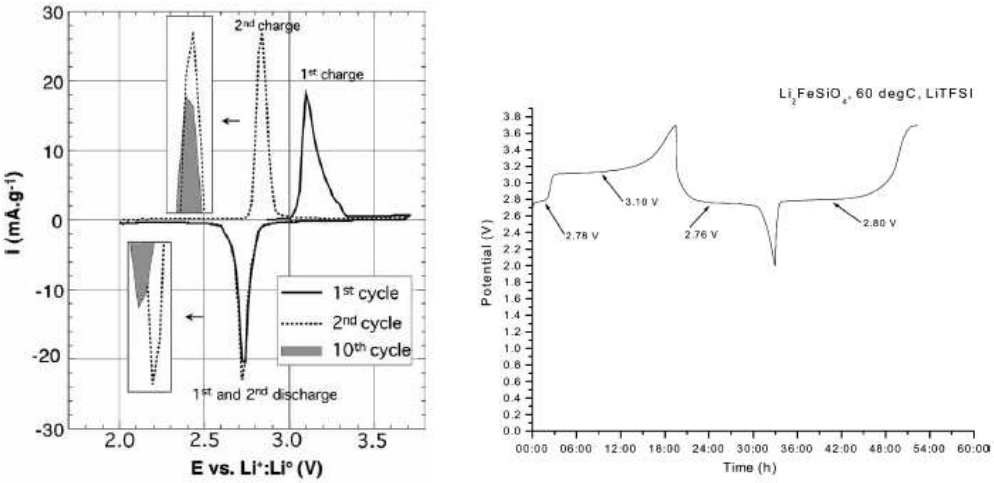

Figure 4

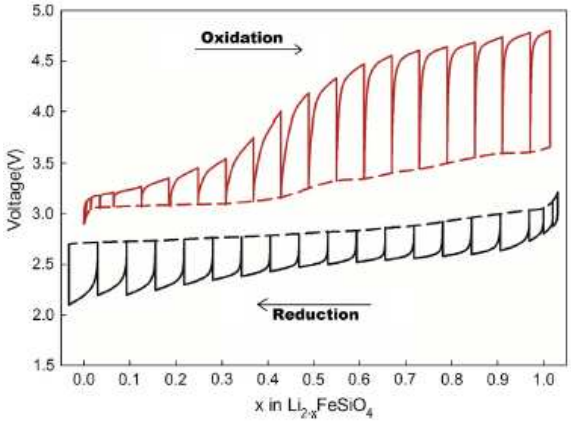

Figure 5

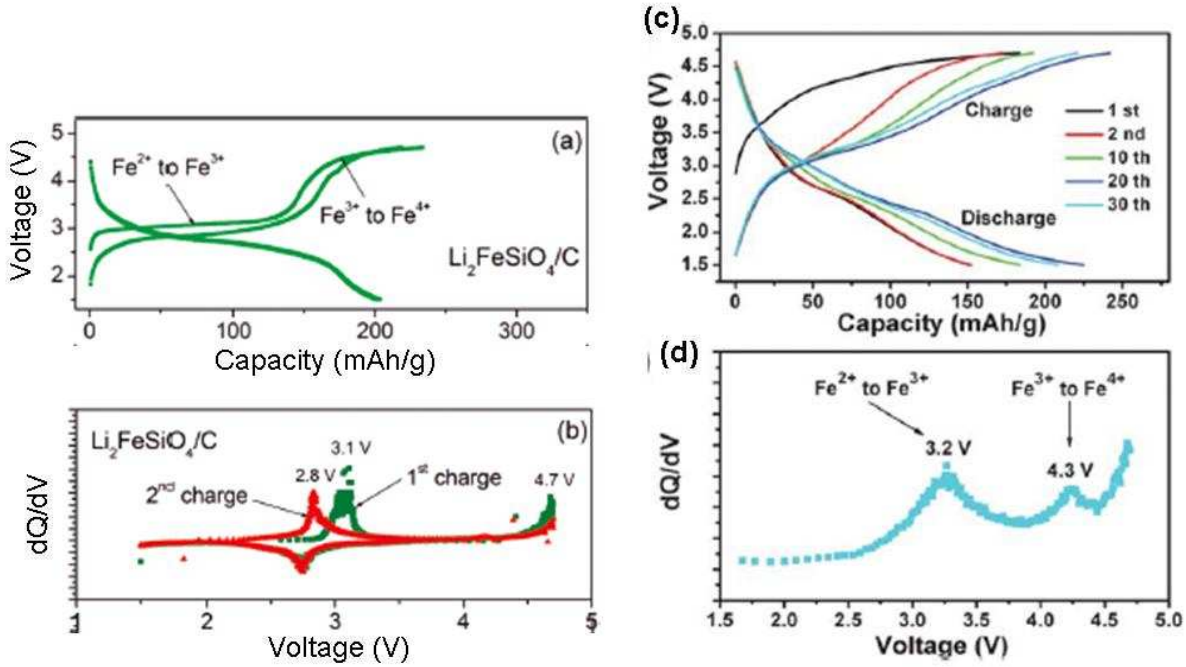

Figure 6

a)

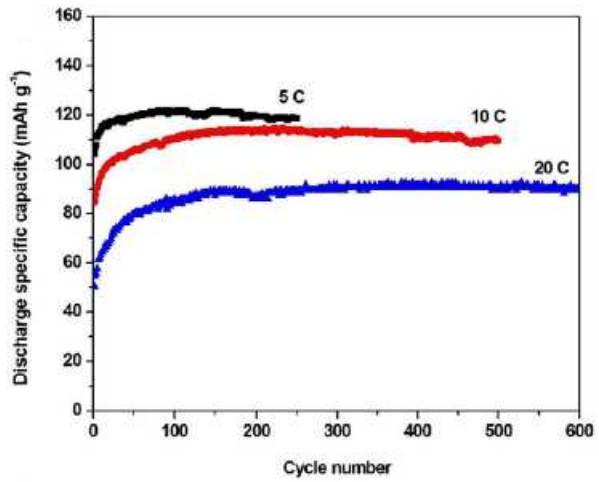

b)

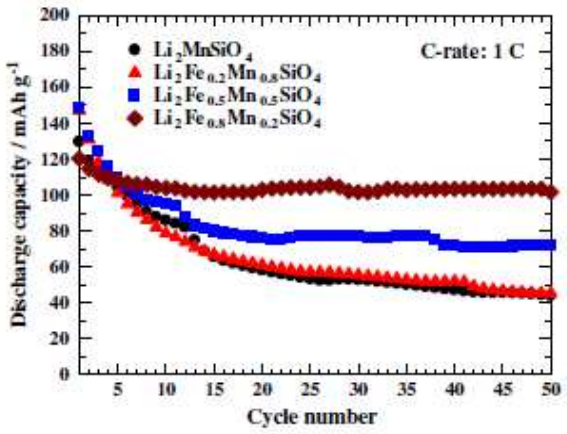

c)

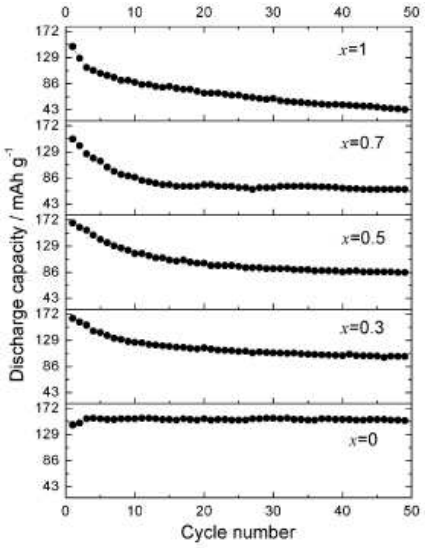

Figure 7

a)

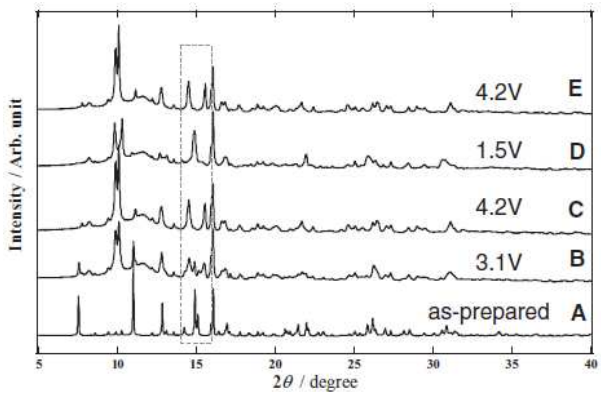

b)

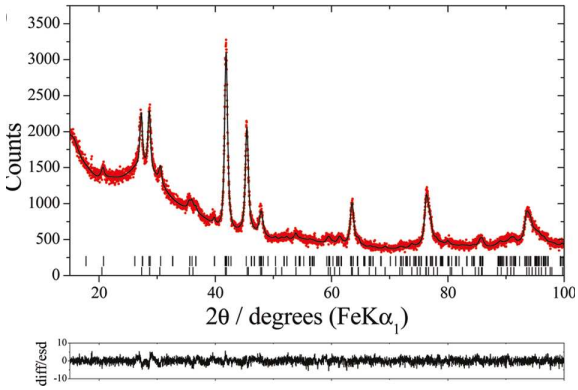

c) d)

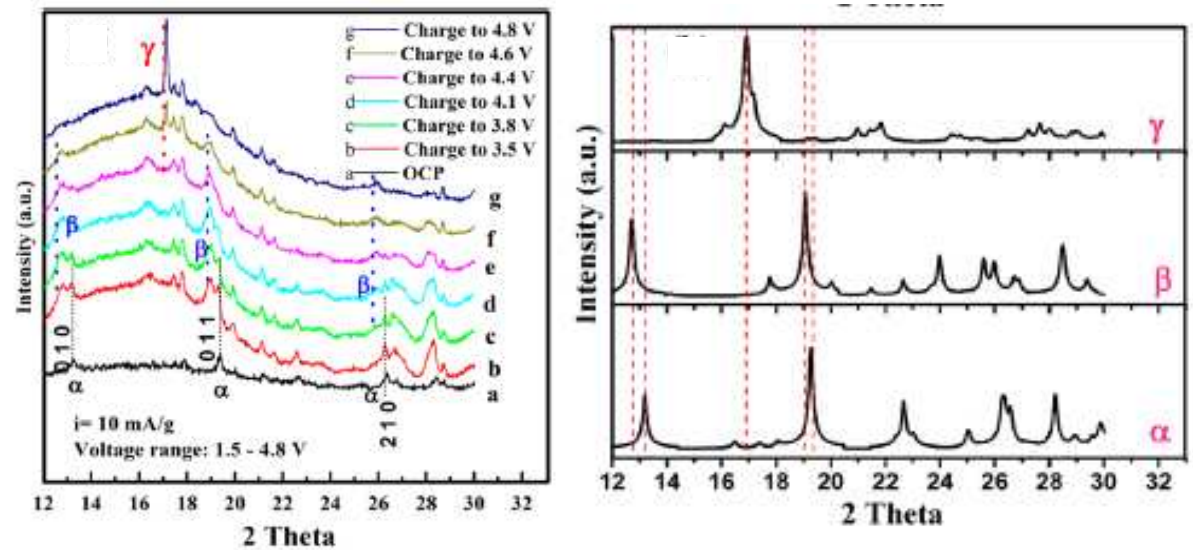

Figure 8

a) b)

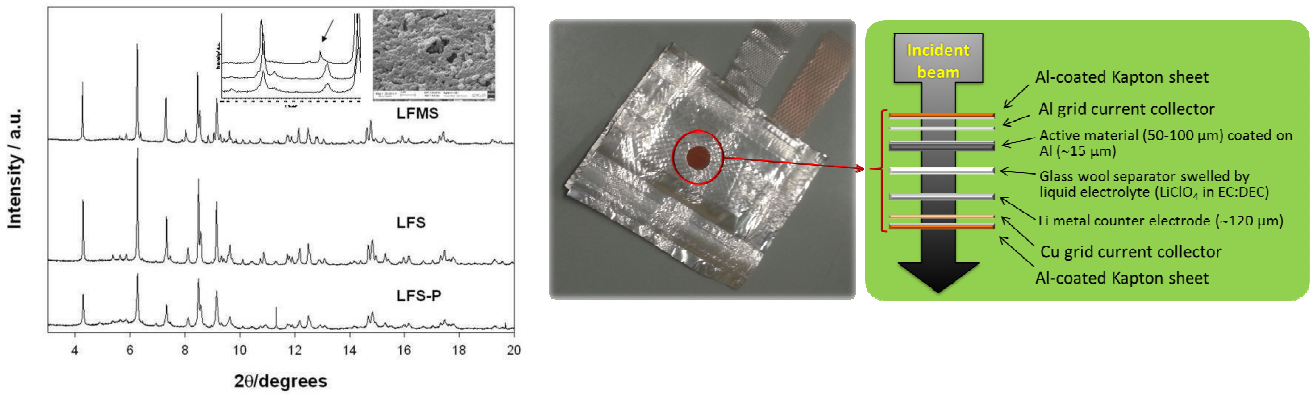

Figure 9

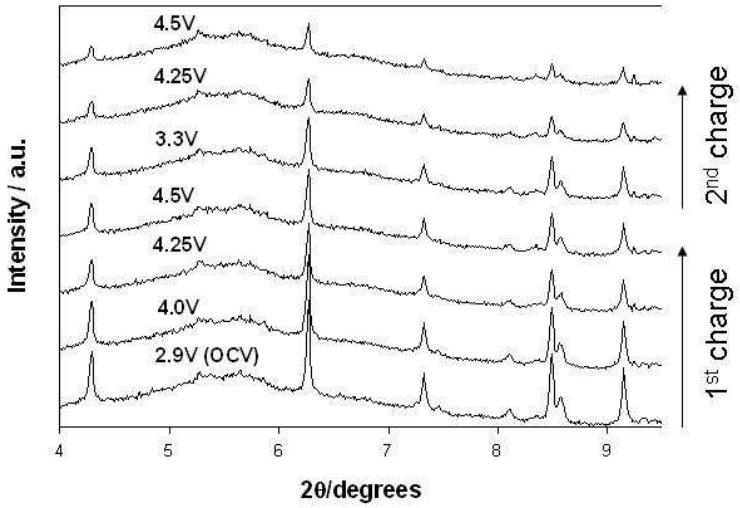

Figure 10

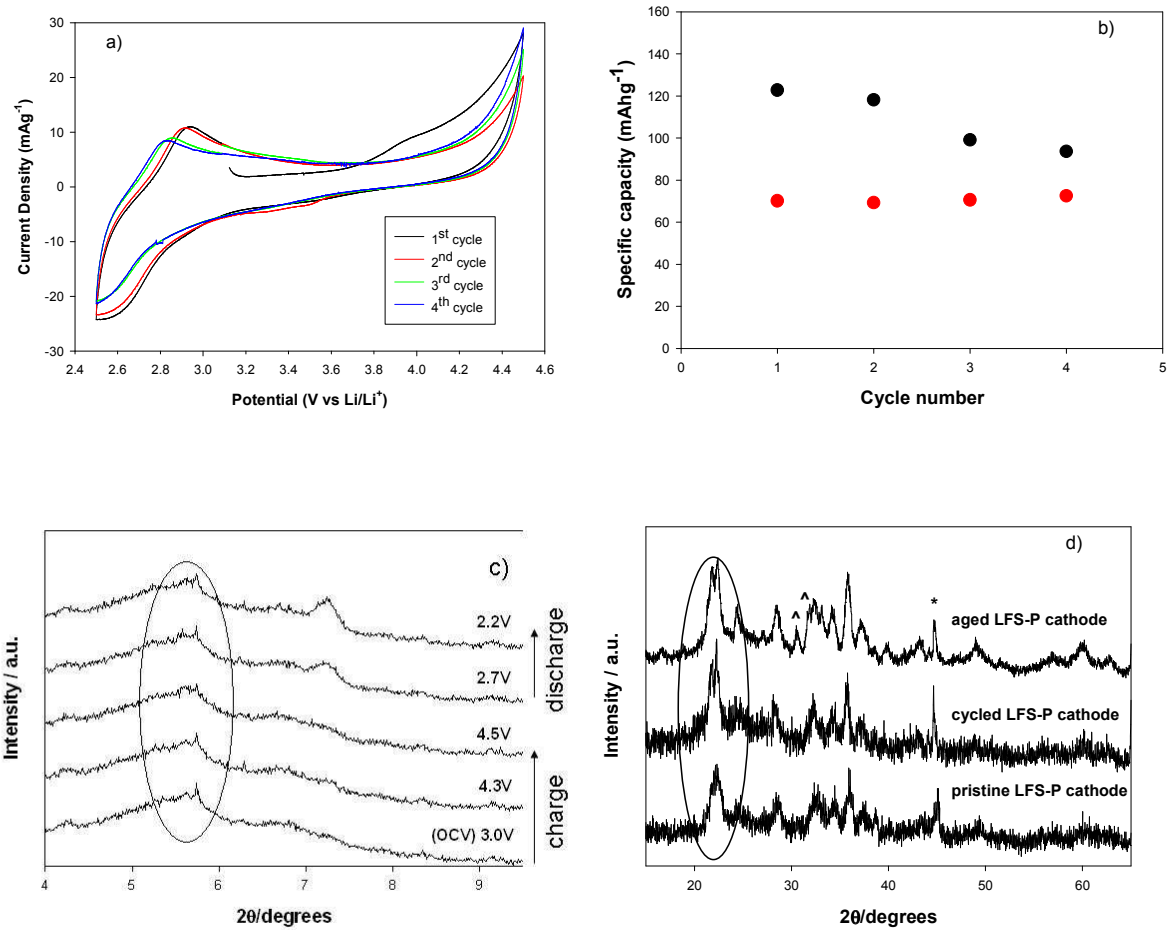

Figure 11